Electron Plasma Orbits from Competing Diocotron Drifts

N. C. Hurst, J. R. Danielson, C. J. Baker, and C. M. Surko
Physics Department, University of California, San Diego, 9500 Gilman Drive, La Jolla, California 92093, USA
(Received 21 April 2014; published 10 July 2014)

The perpendicular dynamics of a pure electron plasma column are investigated when the plasma spans two Penning-Malmberg traps with noncoinciding axes. The plasma executes noncircular orbits described by competing image-charge electric-field (diocotron) drifts from the two traps. A simple model is presented that predicts a set of nested orbits in agreement with observed plasma trajectories.

DOI: 10.1103/PhysRevLett.113.025004 PACS numbers: 52.27.Jt, 41.75.Fr, 52.35.Kt, 52.35.We

Good confinement of single-component plasmas is often realized in a device known as the Penning-Malmberg (PM) trap in which radial confinement is provided by a uniform magnetic field and axial confinement is provided by appropriate voltages on a set of cylindrical electrodes. These devices have been useful for basic plasma physics studies [1,2], and they have been key to advances in the study and use of low-energy antimatter [3–7]. For an azimuthally symmetric trap, conservation of canonical angular momentum limits the plasma expansion [8]. Plasmas in these traps can execute stable, circular $\mathbf{E} \times \mathbf{B}$ drift orbits about the trap axis, known as $m = 1$ diocotron modes, due to image-charge electric fields from the surrounding electrodes. While confinement and equilibria in nonaxisymmetric traps have been studied [9–13], there have been relatively few studies of diocotron-mode dynamics in such traps [14,15].

This Letter describes studies in a nonaxisymmetric electrode structure that results in a new class of noncircular diocotronlike drift orbits. The electrode structure, shown in Fig. 1, provides the capability to move plasmas off the magnetic axis of a large-diameter PM trap (the"master cell") and then allow them to expand along the magnetic field into off-axis traps, referred to here as "storage cells." This configuration, known as a multicell trap, is being investigated as a way to increase antimatter (positron) storage capacity using multiple PM traps in the same vacuum system and magnetic field [16–18]. The results described here are also expected to be useful in advanced scenarios for the production of low-energy antihydrogen [19].

The focus here is on the plasma dynamics for the situation shown in Fig. 1(b), when a plasma spans the master cell and an off-axis storage cell. The image-field drifts in the two cells compete, with each dominant in a particular region of the orbit. The master cell (M) has electrode radius $r_w = 38.0$ mm, while $r_w = 6.0$ mm for the storage cell (S) which is located 30 mm off of the master-cell axis. A third, on-axis cell (A), with $r_w = 8.0$ mm is also used. All PM cells consist of multiple, axially separated cylindrical electrodes, one of which is segmented azimuthally in four equal parts. The entire structure resides in a vacuum of $\sim 10^{-9}$ torr, in a uniform axial magnetic field $B = 4.8$ T. The electron plasmas studied here cool *via* cyclotron radiation in a $1/e$ time of 170 ms.

The initial electron plasmas in the master cell have total numbers $N \sim 1$–2×10^8, temperatures $T \sim 1$ eV, radii $r_p \sim 0.5$–1 mm, lengths $L_p \sim 80$–130 mm, densities 1.2–$1.6 \times 10^{15}\,\mathrm{m}^{-3}$, axial bounce frequencies $f_b \sim 1$ MHz, $\mathbf{E} \times \mathbf{B}$ rotation frequencies $f_r \sim 350$–500 kHz, and diocotron frequencies ~ 100–800 Hz. The plasma parameters in cells A and S are similar, except the diocotron frequencies

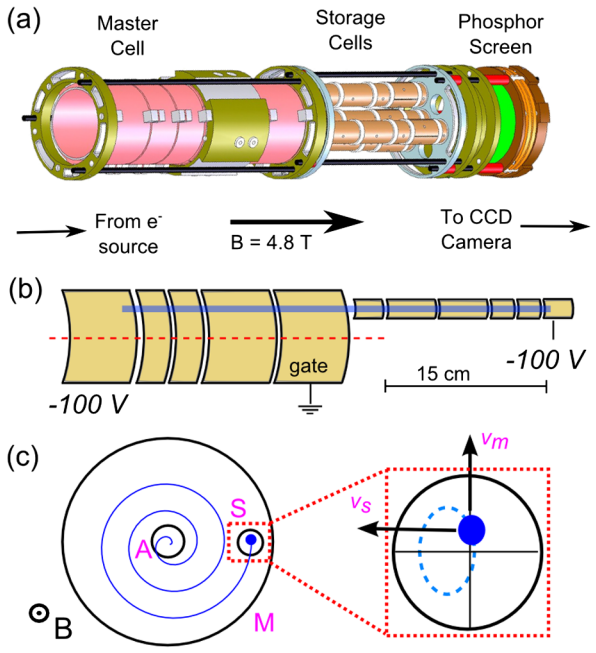

FIG. 1 (color online). (a) Schematic of the experimental apparatus with a master cell and three off-axis and one on-axis storage cells. (b) Electron plasma spanning the master cell and cell S, and (c) outward spiraling trajectory of the plasma in the master cell with a cartoon of the competing diocotron drifts v_m and v_s.

are ~1–3 kHz. Typical expansion times are ~60 s in the master cell, and 10–20 s in the storage cells.

Experiments are conducted in fill-manipulate-image cycles, beginning with the injection of electrons from a heated cathode, on axis, into the master cell. The plasma column is then displaced across B using the autoresonant diocotron drive technique [17,20], resulting in an outward spiraling trajectory such as that shown in Fig. 1(c). When the (r,θ) location of the plasma in the master cell crosses the off-axis location of cell S, the autoresonant drive is turned off, and the confinement-gate electrode separating the two cells is grounded (time $t = 0$), allowing plasma to expand into the storage cell. It is allowed to drift for some time t, at which point the entire plasma is released, accelerated onto a phosphor screen, and imaged using a CCD camera. This provides a destructive diagnostic of the z-integrated electron density $\sigma(r,\theta) = \int dz n(r,\theta,z)$. By varying the delay time t between subsequent shots, the density profile and plasma centroid are tracked to map the $\mathbf{E} \times \mathbf{B}$ drift trajectory of the plasma column.

A key result is that, when the plasma expands axially into this nonaxisymmetric arrangement of two cells, it executes noncircular, but periodic orbits, offset from the center of, and bounded by, the walls of the smaller diameter cell. A typical orbit is shown in Fig. 2 for a plasma spanning the master and off-axis storage cell S. The position at the injection time $t = 0$ is marked by the arrow in the figure. After a brief transient lasting roughly half a cycle (~400 μs), in which the plasma loses some particles to the wall and equilibrates axially, it settles into a stable periodic orbit which is tracked in steps of 50 μs for ~6 cycles spanning ~5 ms. Shown in Fig. 2(c) are the z-integrated plasma density contours $\sigma(r,\theta)$ for a single orbital period after the transient [i.e., the bar in Fig. 2(b)].

As shown in Fig. 3, the plasma motion may also be monitored using the image charge signal on sectored electrodes in the two cells. Prior to $t = 0$, there is a large amplitude diocotron mode with frequency $f \sim 800$ Hz in the master cell. After $t = 0$, the signal from an orbit similar to that of Fig. 2 is detected in the off-axis storage cell. At $t = 5$ ms, the plasma is "cut" at the boundary between the cells by raising the gate voltage, and the signal from the storage cell changes from the slower drift motion into a pure diocotron mode ($f \sim 3$ kHz). The plasma was then dumped at $t = 10$ ms. The large difference in the diocotron frequencies, f_d, between the master cell ($t < 0$) and storage cell ($t > 5$ ms), is due primarily to the dependence of f_d on r_w (discussed below). In contrast, when the plasma spans both cells ($0 < t < 5$ ms), the motion is a competition between these two drifts.

Since the axial bounce frequency is much greater than the diocotron frequency (i.e., $f_b \gg f_d$), the plasma orbits can be described by the axial bounce average of the $\mathbf{E} \times \mathbf{B}$ drifts in the two cells. A simple model, discussed below, predicts a fixed point and a series of nested, closed, periodic orbits, shown in Fig. 2, restricted to the area of the smaller cell S.

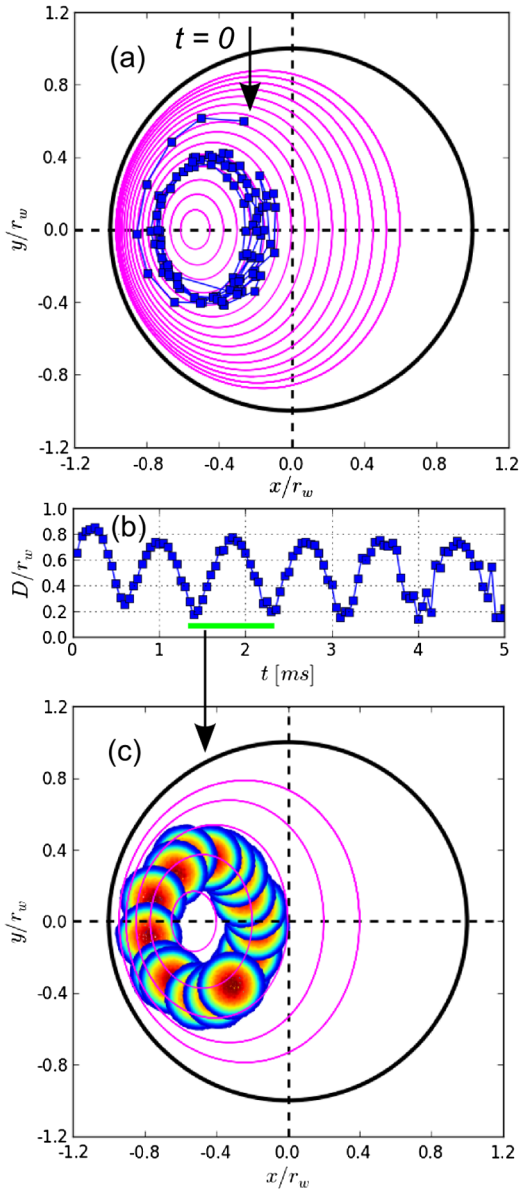

FIG. 2 (color online). Bounce-average orbit of a plasma spanning the master and off-axis cell S, where $r_w = 6.0$ mm is the radius of S, and the master-cell center is at $x = -5.0r_w$. The orbit period is 850 μs. (a) Trajectory of plasma density centroid, (b) centroid displacement D from cell axis vs time, and (c) density contours for one orbit period, with the lowest contour being 5% of the peak density. Also shown in (a) and (c) are expected orbits predicted by a simple model using $\alpha = 0.75$.

The $m = 1$ diocotron mode has been studied extensively for electron plasmas in PM traps [21]. Provided f_b, $f_r \gg f_d$ (typical of the experiments described here), the plasma acts as a rigid line of charge. The nonlinear diocotron frequency for an infinite-length plasma, calculated from the 2D image electric fields, is

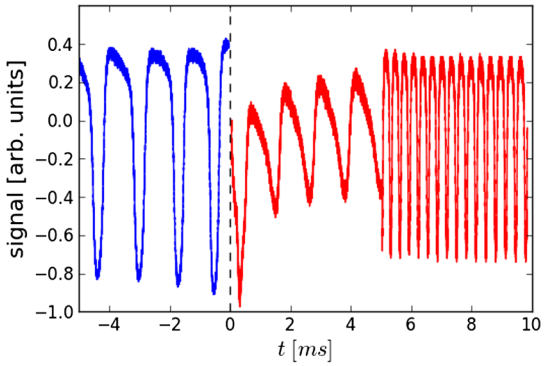

FIG. 3 (color online). Signals from sectored electrodes in the master and cell S during a bounce-averaged orbit. The master cell diocotron mode is observed initially ($t < 0$), then the asymmetric orbit is detected when the gate is grounded ($0 < t < 5$ ms), and, finally, the storage cell diocotron mode is observed after the plasma is cut ($5 < t < 10$ ms).

$$f_d = \frac{f_1}{1-(D/r_w)^2}, \tag{1}$$

where D is the displacement from the axis, and the linear mode frequency is $f_1 = eN/(4\pi^2\epsilon_0 L_p B r_w^2)$.

Finite length corrections to Eq. (1) are important due to the relatively large aspect ratio of the master cell [22]. A detailed model has been constructed that includes nonperturbative finite length effects for large-amplitude modes, the details of which will be published elsewhere [23]. The predictions are in good agreement with the measured diocotron frequencies for $10^8 \leq N \leq 10^9$.

In the model presented here, the total drift of the plasma column is calculated by summing the contributions from both cells,

$$\vec{v} = 2\pi(D_m f_m \hat{\theta}_m + D_s f_s \hat{\theta}_s), \tag{2}$$

where the D_j are plasma displacements, f_j are diocotron frequencies, and $\hat{\theta}_j$ are the azimuthal unit vectors measured in the reference frame of cell j. Since the dynamics are restricted to the area of cell S, a coordinate system centered on it is used, with the center of cell M lying on the negative x axis. Since $|\theta_m| \leq 11^\circ$ over the possible diocotron orbits in cell S, $\hat{\theta}_m$ is taken to be constant, $\hat{\theta}_m = \hat{y}$ in the reference frame of Fig. 2.

The frequencies f_j depend upon the instantaneous number of particles N_j in each cell (i.e., equivalent to calculating the bounce-averaged drift per particle and multiplying by the total number). The N_j are assumed constant in time, which was verified experimentally by taking two CCD images at each time step, one before and one after the plasma is cut, to separate N_m and N_s.

The typical bounce-average orbit trajectory encounters a narrow range of master cell displacements $0.69 \leq D_m \leq 0.76$, that result in only $\sim \pm 10\%$ variation of f_m across the orbit, and so f_m is taken to be constant. In the storage cell, $r_w/L_s < 0.05$ is small enough to neglect finite-length effects, and so Eq. (1) is used to calculate $f_s(D_s)$.

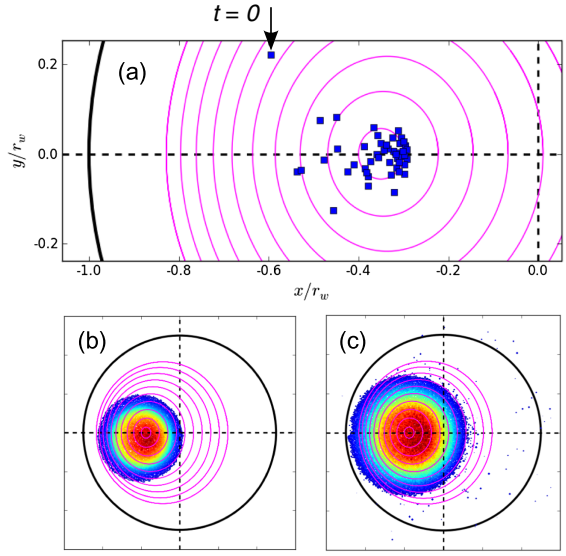

FIG. 4 (color online). (a) A centroid trajectory, corresponding to $\alpha = 0.4$, that remains near the fixed point for ~50 ms; and (b) and (c) density contours at 15 and 45 ms, respectively, showing that the plasma is stable, albeit expanding.

With these assumptions, and in the coordinate system of cell S, the bounce-averaged orbit equation becomes

$$\vec{v}/v_0 = \alpha\hat{y} + \frac{d}{1-d^2}\hat{\theta}, \tag{3}$$

where $d \equiv D/r_w$, $\alpha \equiv v_y/v_0$ with $v_y \equiv 2\pi D_m f_m$ (i.e., the master cell diocotron drift velocity), and $v_0 = 2\pi f_1 r_w$ evaluated for the storage cell. The parameter α, which is the ratio of the master cell to storage cell drift, uniquely determines a set of nested orbits corresponding to different initial conditions in the (r, θ) plane at $t = 0$. Such orbits are shown in Figs. 2(a) and 2(c), with α chosen to fit the data.

There is a fixed point of Eq. (3) (the solution to $\vec{v} = 0$), which lies on the x axis ($y = 0$) at

$$x = -(2\alpha)^{-1}(\sqrt{1+4\alpha^2} - 1). \tag{4}$$

The initial transient causes the plasma to cross orbits (i.e., Hamiltonian preservation is violated for $t \lesssim 500$ μs), and so, to approach this point, the initial condition must be chosen such that the transient orbit-crossing behavior ends as the trajectory approaches the fixed point. This is demonstrated in Fig. 4, where the position at $t = 0$ is identified by an arrow. The plasma expands and loses particles to the wall within the first 1 ms, then settles into a long-lived state near the fixed point featuring expansion and particle loss on a much longer time scale (at least 50 ms).

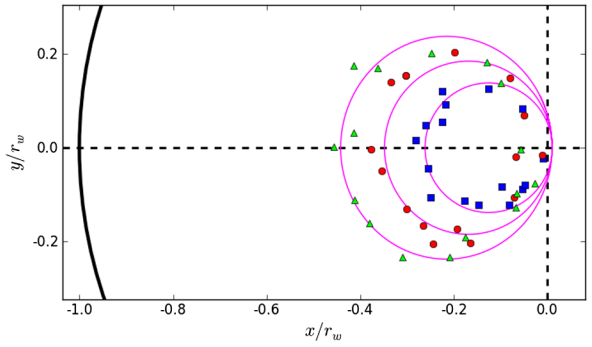

FIG. 5 (color online). Asymmetric orbit trajectories in a single cell for V_1 =(square) 5, (circle) 8, and (triangle) 10 V. The orbital periods are ~400–450 μs. Also shown are the predictions of Eq. (3) with $\alpha = 0.13, 0.18, 0.24$, respectively.

Similar orbits to that of Eq. (3) are expected if a uniform transverse electric field is applied directly in a single storage cell. This was tested, and the results shown in Fig. 5 verify that this is indeed the case. With a plasma confined solely in cell A (the on-axis storage cell), a static transverse electric field is created at $t = 0$ by rapidly applying a voltage V_1 (e.g., $\Delta t \leq 10$ μs) to a 180° portion of the electrodes, leaving the other 180° portion grounded. The resulting orbit data are shown in Fig. 5, for the plasma initially located near the axis of cell A, for three values of V_1. Increasing V_1 increases α, and thus moves the stationary point further from the symmetry axis. Fits to the data using Eq. (3), shown in Fig. 5, are in good agreement with the measurements, thus confirming the validity of the model for this situation also. Similar behavior has been investigated by Chu *et al.* [15].

The values of α and v_0 in Eq. (3) can be predicted from the measured values of N_m and N_s (or V_1 and N_s in the case of a single-cell orbit) and calculation of the finite-length diocotron frequencies. They can also be obtained by using the model to fit the orbit shape (for α) and orbit period (for v_0 at fixed α). The approximate parameter values for the data shown in Fig. 2 are $N_m = 6.5 \times 10^7$, $N_s = 5.5 \times 10^7$, $L_m = 0.19$ m, and $L_s = 0.17$ m. The predicted (model fit) values are $\alpha = 0.32\,(0.75)$, and $v_0 = 32\,(23)$ m/s. For the data in Fig. 5 and $V_1 = 8$ V, $\alpha = 0.19\,(0.18)$, and $v_0 = 74\,(112)$ m/s. Reasons for the discrepancies include possible additional physics in the process of cutting the plasma or at the boundary between the two cells, the validity of the finite-length diocotron frequency model for low N/L, and assumptions made regarding the bounce-average dynamics.

It is shown here that, for a plasma spanning multiple PM traps with displaced symmetry axes, the competition between naturally occurring drifts results in stable, periodic, bounce-averaged orbits. These orbits are expected to be useful for plasma transfer into off-axis cells of a multicell trap [17,18], since transfer times can be extended to tens of milliseconds, as opposed to ~50 μs if the master-cell dynamics were to dominate.

The equilibria and dynamics of the orbits described here are related to other phenomena, including an asymmetric $m = 1$ equilibrium plasma position that corresponds to the stationary point of Eq. (3) [9], the adiabatic invariance of the area enclosed by a noncircular drift orbit [14], equilibria in PM traps with large static asymmetries [11,15,20], and varying the size of a magnetron orbit in a Penning trap using a transverse electric field [24]. Finally, pure-lepton plasma dynamics are closely related to ideal, 2D fluid dynamics. The z-dependent dynamics described here are similar to the motion of a vortex or cyclonic structure in a vertically sheared flow [25].

We thank Gene Jerzewski for expert technical assistance. This work was supported by the U.S. Defense Threat Reduction Agency.

[1] D. H. E. Dubin and T. M. O'Neil, Rev. Mod. Phys. **71**, 87 (1999).
[2] *Nonneutral Plasmas VIII*, edited by X. Sarasola, L. Schweikhard, and T. S. Pedersen(American Institute of Physics, Melville, NY, 2013), Vol. 1521.
[3] C. M. Surko and R. G. Greaves, Phys. Plasmas **11**, 2333 (2004).
[4] M. Amoretti *et al.*, Nature (London) **419**, 456 (2002).
[5] G. Gabrielse, N. S. Bowden, P. Oxley, A. Speck, C. H. Storry, J. N. Tan, M. Wessels, D. Grzonka, W. Oelert, G. Schepers, T. Sefzick, J. Walz, H. Pittner, T. W. Hasch, and E. A. Hessels, Phys. Rev. Lett. **89**, 233401 (2002).
[6] G. B. Andresen *et al.*, Phys. Rev. Lett. **105**, 013003 (2010).
[7] D. B. Cassidy and A. P. Mills, Nature (London) **449**, 195 (2007).
[8] T. M. O'Neil, Phys. Fluids **23**, 2216 (1980).
[9] J. M. Kriesel, Ph.D. Thesis, University of California, San Diego, unpublished, 1999.
[10] J. Fajans, E. Y. Backhaus, and J. E. McCarthy, Phys. Plasmas **6**, 12 (1999).
[11] E. Y. Backhaus, J. Fajans, and J. S. Wurtele, Phys. Plasmas **6**, 19 (1999).
[12] J. Notte and J. Fajans, Phys. Plasmas **1**, 1123 (1994).
[13] J. M. Kriesel and C. F. Driscoll, Phys. Rev. Lett. **85**, 2510 (2000).
[14] J. Notte, J. Fajans, R. Chu, and J. S. Wurtele, Phys. Rev. Lett. **70**, 3900 (1993).
[15] R. Chu, J. S. Wurtele, J. Notte, A. J. Peurrung, and J. Fajans, Phys. Fluids B **5**, 2378 (1993).
[16] C. M. Surko and R. G. Greaves, Radiat. Phys. Chem. **68**, 419 (2003).
[17] J. R. Danielson, T. R. Weber, and C. M. Surko, Phys. Plasmas **13**, 123502 (2006).
[18] J. R. Danielson, N. C. Hurst, and C. M. Surko, in *10th International Workshop on Non-Neutral Plasmas*, Vol. Nonneutral Plasmas VIII, edited by X. Sarasola, L. Schweikhard, and T. S. Pedersen (American Institute of Physics, Greifswald, Germany, 2013), p. 101.
[19] C. Canali, C. Carraro, D. Krasnicky, V. Lagomarsino, L. D. Noto, G. Testera, and S. Zavatarelli, Eur. Phys. J. D **65**, 499 (2011).

[20] J. Fajans, E. Gilson, and L. Friedland, Phys. Plasmas **6**, 4497 (1999).
[21] R. J. Briggs, J. D. Daugherty, and R. H. Levy, Phys. Fluids **13**, 421 (1970).
[22] K. S. Fine and C. F. Driscoll, Phys. Plasmas **5**, 601 (1998).
[23] N. C. Hurst *et al.* (unpublished).
[24] T. Mortensen, A. Deller, C. A. Isaac, D. P. Van der Werf, M. Charlton, and J. R. Machacek, Phys. Plasmas **20**, 012124 (2013).
[25] R. K. Smith, W. Ulrich, and G. Sneddon, Q. J. R. Meteorol. Soc. **126**, 2653 (2000).